Three-Dimensional Finite-Difference Method for the Analysis of Microwave-Device Embedding

ANDREAS CHRIST AND HANS L. HARTNAGEL, SENIOR MEMBER, IEEE

Abstract—**The embedding of microwave devices is treated by applying the finite-difference method to three-dimensional shielded structures. A program package was developed to evaluate electromagnetic fields inside arbitrary transmission-line connecting structures and to compute the scattering matrix. The air bridge, the transition through a wall, and the bond wire are examined as interconnecting structures. Detailed results are given and discussed regarding the fundamental behavior of embedding.**

I. INTRODUCTION

THE EMBEDDING PROBLEM is concerned with the interconnection of an active semiconductor device, such as a diode, an FET, or an MIC, with the electrical surroundings where one considers both electrical and mechanical aspects. Especially at frequencies up to 100 GHz, with monolithic integrated millimeter-wave circuits, the design of embedding structures becomes important. The high permittivity of the semiconductor materials promotes field distortions at such structures. From a mechanical point of view, the handling, the stability, the protection against environmental factors, and the feasibility of fabricating a device and its connecting structure have to be considered. They influence the package geometry and therefore also the electrical characteristics of the active device.

Embedding is not only significant inside packages, as often required for protection, but also when these components are directly bonded into microstrip or other lines.

Electrically, the embedding can be regarded as the interconnection of two or more transmission lines, which may be waveguides, coaxial lines, dielectric image guides, microstrip lines, or slotlines, using a connecting structure (Fig. 1).

This is in general a multiport scattering problem and can be described by the generalized scattering matrix.

The requirements are a small reflection coefficient and a linear phase of the transmission coefficient in the frequency range of interest. A zero point of the reflection coefficient should be looked for in analog applications where the relative bandwidth is usually small. For the digital case, the interconnection has to be broad-band from zero up to several gigahertz because of the appearance of harmonics and to avoid pulse widening.

To describe the electrical behavior, most authors have used lumped-element circuits. Getsinger divided the lumped-element circuit into two parts, one representing the package, the other the mount [1]. The parameters of some diode packages were measured, and the parameters for mounting into waveguide, strip, and coaxial line were calculated using an approximating theory. Bialkowski and Khan calculated the driving-point impedance for diodes in waveguides and similar lines [2]. They verified their results by measurements. Maeda *et al.* [3] measured all parameters for an embedded laser diode. A general measurement method without the need of reference packages was presented by Greiling and Laton [4], but they could not distinguish the packaging and mounting parts. Their method was applied to diodes but could also handle other devices.

The parasitic reactances of two microwave transistor packages (LID and S2) mounted in microstrip were measured by Akello *et al.* [5] using the resonance method. In particular, the inductance of the bond wires as a function of wire spacing and number was examined. Typical values for LID were 0.61 nH to 0.76 nH (one wire). Beneking presented slightly different values (0.2 nH to 0.5 nH) obtained by a time-domain measurement technique for small reactances and susceptances [6].

The available values are mostly based on measurements and are restricted to some commonly used but special packages. Although Akello *et al.* demonstrated an important influence on the device characteristics, such as gain and stability factor [5], there has until now been no fundamental analysis to find well-matched structures. Therefore, a numerical method able to examine embedding structures is given in this paper and some of the significant results are presented here. In general, the geometry of such structures forces a three-dimensional analysis of the electromagnetic fields, and the expected frequency range for microwave applications needs the rigorous numerical solution of Maxwell's equations.

However, the numerical methods tested to handle scattering problems by finding the scattering matrix, a frequency-domain problem, often exhibit some lack of generality. The spectral-domain approach [7] can only be applied to planar structures. The method of moments, requiring a knowledge of the Green's function, is practi-

Manuscript received November 28, 1986; revised April 1, 1987. This work was supported in part by the Deutsche Forschungsgemeinschaft.

The authors are with the Institut für Hochfrequenztechnik, Technische Hochschule Darmstadt, 6100 Darmstadt, West Germany.

IEEE Log Number 8715144.

0018-9480/87/0800-0688$01.00 ©1987 IEEE

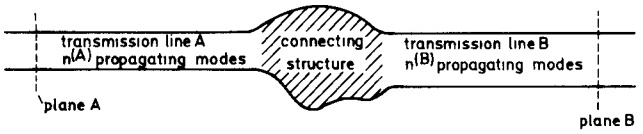

Fig. 1. General structure under view.

cally applicable to planar structures or inside waveguides [8]–[11]. Orthogonal expansions in view of mode matching can be applied to transmission-line connections [12], [13].

The finite-element method allows arbitrary structures and has been tested by Webb, Maile, and Ferrari [14] and de Pourcq [15]. They allowed only one propagating mode far away from the scattering object.

Finally, the finite-difference method is frequently used for solving the time-dependent Maxwell's equations [16] and its eigenvalue problem in connection with both transmission-line characteristics, e.g. [17]–[19], and three-dimensional cavity resonator problems [17], [18], [20]–[22]. The publications relevant to the following work are given here. As will be shown, the scattering matrix can be calculated if the three-dimensional boundary value problem can be solved. Because the finite-difference method is a powerful one, it has been selected here. The structure geometry can be chosen nearly arbitrarily, and filling materials having arbitrary complex permittivity and permeability are allowed. Further, this method has been well tested in connection with cavity resonator problems. To the best knowledge of the authors, this method has not been applied before to the above problem.

Firstly, the evaluation of the scattering matrix and the basic ideas of the finite-difference method are described. Then some testing structures are presented. Finally, numerical results of embedding structures are discussed and some concluding remarks are added.

II. Evaluation of the Scattering Matrix

Two or more infinitely long, longitudinally homogeneous, but in general different, transmission lines are attached to the connecting structure. The complex generalized scattering matrix S describes the energy exchange and phase relation between all outgoing modes (b_k) and all incoming modes (a_l). It is of infinite order but in practice is limited to the order n if on any transmission line only a finite number of modes are considered:

$$S = \begin{pmatrix} S_{11} & S_{12} & \cdots \\ S_{21} & & \\ \vdots & S_{kl} & \end{pmatrix}, \qquad 1 \leqslant k, l \leqslant n \tag{1a}$$

$$S_{kl} = \left.\frac{b_k}{a_l}\right|_{\substack{\forall \\ l \neq k}\ a_l = 0} \qquad a_l, b_k\text{: mode amplitudes.} \tag{1b}$$

The indices l and k have to be chosen in such a way that all n modes under consideration at all transmission lines are numbered but no conflicts occur.

When one goes away from the connecting structure, the energy of the evanescent and complex modes decreases exponentially. Therefore the number of modes relevant within the limits of accuracy also decreases with distance until finally only propagating modes have to be taken into account.

The basic principle used here to obtain the scattering matrix is as follows. The scattering matrix can be calculated if an orthogonal decomposition of the electrical field is known at two neighboring planes—one pair on each transmission line—and if it is known for a sufficient number of linear independent exitations on these transmission lines.

Therefore, the electric field is required. For its numerical calculation, both the connecting structure and the infinitely long transmission lines are first shielded by an envelope. Then, each transmission line and the envelope around it are cut at cross-sectional planes p. This means that a boundary value problem is built up and that the electric field inside is uniquely determined if the transverse electric field is known on the whole surface.

At the cross-sectional planes, the transverse electric field $\vec{E}_t^{(p)}$ is given by superposing all normalized transmission-line modes with mode-amplitude sums $w_i^{(p)}$:

$$\vec{E}_t^{(p)} = \sum_{i=1}^{n_{\text{mod}}^{(p)}} w_i^{(p)} \cdot \vec{E}_{ti}^{(p)}, \qquad n_{\text{mod}}^{(p)}\text{: number of modes taken into account at plane } p. \tag{2}$$

The transverse-mode fields $\vec{E}_{ti}^{(p)}$ are normalized and satisfy the orthogonality relation [23]

$$\int_A \vec{E}_{ti}^{(p)} \times \vec{H}_{tj}^{(p)} d\vec{A} = \delta_{ij} \tag{3}$$

where δ_{ij} is the Kronecker symbol, and $\vec{E}_{ti}^{(p)}$ and $\vec{H}_{tj}^{(p)}$ are mode fields, in general complex. This is important if higher modes and/or different transmission lines are considered.

At the envelope, i.e., at all other parts of the surface, the transverse electric field is assumed to equal zero. This is similar to most practical microwave applications where the circuits are shielded by a metal.

The mode amplitudes a_i and b_i are determined if the boundary value problem has been solved. for this, the orthogonality relation (3) is applied at two neighboring planes cutting the longitudinal transmission-line axis at z_p and $z_p + \Delta_z$, $|\Delta_z|$ being their separation. Thus, one obtains the following mode-amplitude sums w_i:

$$\int_A \vec{E}_t(z_p) \times \vec{H}_{ti}^{(p)} d\vec{A} = a_i(z_p) + b_i(z_p) = w_i(z_p) \tag{4a}$$

$$\int_A \vec{E}_t(z_p + \Delta_z) \times \vec{H}_{ti}^{(p)} d\vec{A} = a_i(z_p + \Delta_z) + b_i(z_p + \Delta_z) = w_i(z_p + \Delta_z). \tag{4b}$$

Usually, one of the two neighboring planes is identical to the cross-sectional plane p. Therefore, $w_i(z_p) = w_i^{(p)}$ and

is known because its value is given. Now the relations

$$a_t(z_p+\Delta_z)=a_t(z_p)\cdot e^{\mp\gamma_t^{(p)}\cdot\Delta_z} \tag{5a}$$

$$b_t(z_p+\Delta_z)=b_t(z_p)\cdot e^{\pm\gamma_t^{(p)}\Delta_z} \tag{5b}$$

are used to eliminate $a_t(z_p+\Delta_z)$ and $b_t(z_p+\Delta_z)$ in (4b) and to obtain the mode amplitudes $a_t(z_p)$ and $b_t(z_p)$. Here, $\gamma_t^{(p)}$ are the propagation constants of the transmission-line modes being considered. Their sign has to be chosen depending on whether the $+z$ direction goes toward or away from the connecting structure.

In order to fully evaluate the generalized scattering matrix of order n,n solutions of the boundary value problem with linearly independent boundary conditions are necessary, i.e., different $\vec{E}_t^{(p)}$ at the cross-sectional planes p. The reason for this is that the scattering matrix is composed of $n\cdot n$ complex coefficients; thus, the same number of complex equations has to be built up. Based on the solution of one boundary value problem, one equation is extracted for every outgoing mode, combining its amplitude with those of all incoming modes; this means that n (linear, complex) equations are found. Therefore, $n\cdot n/n = n$ different boundary value problems have to be solved.

III. Finite-Difference Method

The basic ideas of the finite-difference method are described here as applied to the solution of the boundary value problem and the calculation of the scattering matrix.

The bounded region is divided into elementary cells by using a three-dimensional nonequidistant Cartesian grid along which it is cut. Therefore, the bounded region is a rectangular box in its simplest case. The electric field components are defined at the central points of the corresponding edges of the elementary cells, i.e., the E_{mx} component at an edge parallel to the x axis, etc. The magnetic field components are defined at the central points of the corresponding surfaces of the elementary cells, but perpendicular to the surfaces. This builds up a dual grid (Fig. 2) [16], [18].

Because a rigorous full-wave treatment is necessary at high frequencies, Maxwell's equations are used. To obtain a linear equation system for the defined field components, their integral form in the frequency domain is applied:

$$\oint_C \vec{H}\cdot d\vec{s}=\int_A j\omega\epsilon\vec{E}\cdot d\vec{A}+\int_A \vec{J}_e\cdot d\vec{A} \tag{6a}$$

$$\oint_C \vec{E}\cdot d\vec{s}=-\int_A j\omega\mu\vec{H}\cdot d\vec{A} \tag{6b}$$

and the fields are approximated by three-dimensional step functions. The defined $\vec{H}$ field components in the discrete region are expressed by the surrounding $\vec{E}$ field by applying (6b) to the surfaces of the elementary cells. The same can be done with the $\vec{E}$ field components using the dual grid and taking the current source $\vec{J}_e$ into account (6a). The elimination of the $\vec{H}$ field components leads to a set

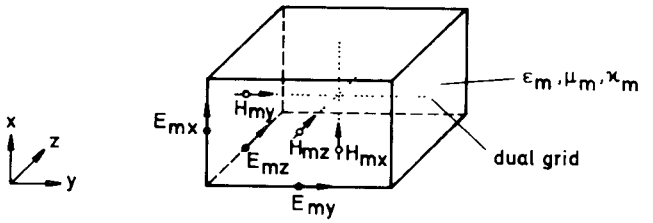

Fig. 2. Elementary cell of the finite-difference method.

of linear equations [18] where every E_{mq} is a function f_{mq} of 12 neighboring $\vec{E}$ field components $E_{m_kq_k}$:

$$E_{mq}=f_{mq}\left(E_{m_kq_k}\right),\qquad 1\leqslant k\leqslant 12 \tag{7}$$

m, m_k: number of cell

$q, q_k \in \{x, y, z\}$.

The Maxwell equations

$$\oint_A \epsilon\vec{E}\cdot d\vec{A}=0 \tag{8a}$$

$$\oint_A \mu\vec{H}\cdot d\vec{A}=0 \tag{8b}$$

are satisfied using the grid mentioned above for all defined components [18]. The cells are filled with ϵ_m, μ_m and may have a conducting property κ_m. Tensors for ϵ_m, μ_m are allowed as far as the main axes are parallel to the coordinate axes [18]. Every cell can be divided into two half cells by a diagonal plane to get a better approximation of the material boundaries inside and of the envelope [19].

The set of equations which one obtains if all electric field components inside and on the boundary are considered can be written as an inhomogeneous system of linear equations:

$$M\cdot\vec{e}=\vec{b} \tag{9a}$$

$$M=M(\epsilon_m, \mu_m, \kappa_m, d_q, \omega) \tag{9b}$$

where d_q is the grid distance, $\omega=2\pi f$ is the angular frequency, and M is a sparse but not symmetric matrix describing the structure. If well designed, its dimension is three times the number of elementary cells, but only 25 diagonals contain values different from zero. Here, $\vec{e}$ is a vector with all electric field components inside and some on the boundary, and $\vec{b}$ is the vector containing the values of the sources inside and the transverse field components on the boundary. These transverse field components are calculated as described in Section II.

After having solved the linear system of equations (9a), the electric field is used to calculate the mode amplitudes. In this application, the neighboring planes are placed at the distance of one grid step. One of them is the cross-sectional plane which is a boundary of the region.

Finally, the system of linear equations involved with the scattering-matrix coefficients is solved by a standard routine.

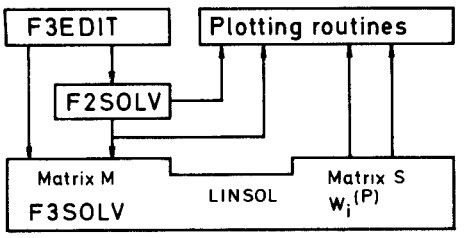

Fig. 3. Data transfer in the program package F3D.

IV. Implementation

The program package F3D divided into four logical blocks has been implemented (Fig. 3). F3EDIT allows the construction and changing of 3-D structures in an interactive manner. It also has the ability to prepare and change the control data for F2SOLV and F3SOLV. To calculate the propagation constants $\gamma_i^{(p)}$ and the transverse electric mode fields $\vec{E}_{ti}^{(p)}$ of the (in general) transverse inhomogeneous transmission lines, F2SOLV has to be called up. It also applies to the finite-difference method as basically described in [18] but contains a standard eigenvalue solver finding all propagation constants and a Gauss elimination procedure with pivot searching on a section of the main diagonal for determination of $\vec{E}_{ti}^{(p)}$ under consideration. The fields are normalized using (3) in its discrete form.

The kernel of the program package, F3SOLV, mainly contains the evaluation procedure of the matrix M, the linear-equation solver, and the algorithm to determine the scattering matrix. As linear-equation solver, several iterative methods are available in the program package LINSOL [24], specially implemented for large sparse asymmetrical matrices stored in a diagonal manner. Having the best convergence behavior for the application presented, the biconjugate gradient method [25] was used. The version of F3SOLV implemented has some restrictions due to programming simplification. The filling material has to be isotropic and source free. Also, losses are not allowed to reduce the complex inhomogeneous system (9a) to a real one. Therefore, the electric field inside is real if real boundary conditions are forced; i.e., $\vec{E}$ is a summation of standing waves and evanescent fields. Further, the elementary cells cannot be divided into half cells and the transmission lines are connected at opposite sides. These restrictions are chosen in considering the applications for which the program is intended. They are not basic restrictions.

The mode-amplitude sums of interesting modes can be stored by numerical decomposition of the evaluated fields along longitudinal homogeneous parts of the structure (4a). This makes it possible to examine the excitation of modes near scattering regions. The S-matrix algorithm is called up after a sufficient number of runs have been executed with different boundary values.

Some plotting routines are added to draw transverse mode fields and their propagation constants, mode-amplitude sums, and scattering coefficients.

Because of the large number of elementary cells necessary to build up a three-dimensional structure and therefore because of the large number of linear equations which have to be solved, F3SOLV was implemented on a vector computer, the CYBER 205. Some typical elementary cell numbers and computing times are given in Table I for several of the structures examined here.

TABLE I
CPU Time of F3SOLV for the Scattering Matrix Calculation at One Frequency Point

Structure	Fig.	Number of elementary cells vertical × horizontal × longitudinal	Number of equations	CPU time of F3SOLV
Partially filled coaxial line	4	6×10×84 equidistant grid	15120	20 s
Dielectric scattering obstacle; $d = 0.8 \cdot a$	6	5×10×88 nonequidistant grid	13200	16 s
Dielectric wall; $\epsilon_{rw} = 9.8$ $d = 12.7 \cdot a$	10	8×10×92 nonequidistant grid	22080	56 s
Bond wire; $d = 12.7 \cdot a$	17	10×12×96 nonequidistant grid	34560	174 s

V. Testing Structures

To estimate the accuracy of the method described, several structures have been considered.

Regarding longitudinally homogeneous structures, the error of the phase of the transmission coefficient increases linearly with the structural length, normalized to the wavelength, and quadratically with the grid distances in the longitudinal direction, also normalized to the wavelength. The error of the magnitude of the reflection coefficient shows a more complicated, but basically similar, behavior.

Regarding single transversal or longitudinal material boundaries, the error depends on the grid used in its neighborhood. The observed values of the error of the magnitude were $\Delta|S_{11}| \leqslant 0.015$ by comparison with a finer grid net.

To give a further idea of the accuracy, some plots which compare the results with those of other methods are given. In the following plots, the magnitude of the reflection coefficient, $|S_{11}|$, is plotted via the normalized frequency $a \cdot k_0 = a \cdot 2\pi f \cdot \sqrt{\epsilon_0 \mu_0}$, with a being the length-normalization constant. Because of the losslessness of the structures, the magnitudes of the other S-matrix coefficients contain no further information ($|S_{22}| = |S_{11}|$; $|S_{12}| = |S_{21}| = \sqrt{1 - |S_{11}|^2}$). All structure dimensions are also normalized to a.

Fig. 5 shows $|S_{11}|$ of a coaxial line partially but transverse homogeneously filled with a dielectric ($\epsilon_r = 9$) (Fig. 4). The dotted line represents the exact values obtained by analytical considerations. The agreement is very good, indicating the correctness of the chosen method.

A dielectric scattering obstacle placed in a waveguide was examined by Katzier [13], who applied the mode-

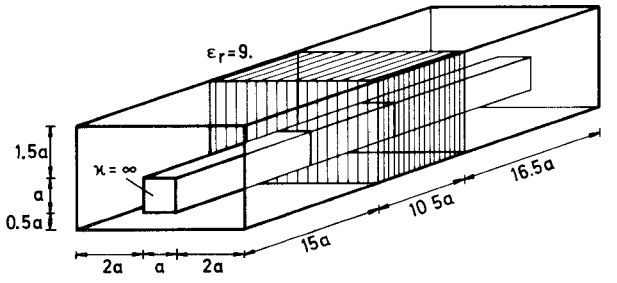

Fig. 4. Rectangular coaxial line partially filled with a dielectric.

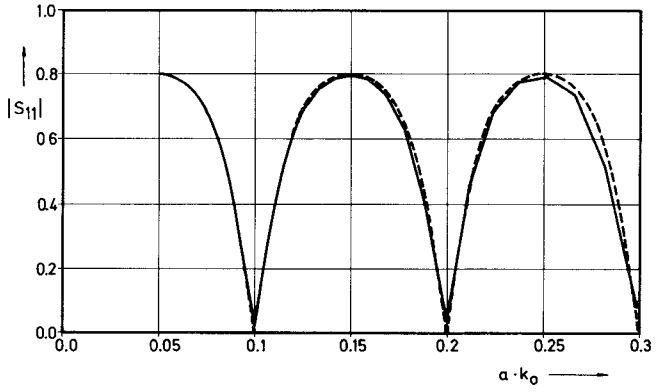

Fig. 5. Magnitude of the reflection coefficient $|S_{11}|$ of the structure of Fig. 4. —— finite-difference method. ----- analytical calculations.

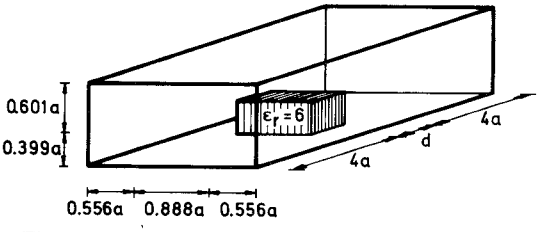

Fig. 6. Dielectric scattering obstacle in a waveguide.

matching method using orthogonal expansions. This has been recalculated with the technique described in this paper (Fig. 6). The curves show a good matching of both methods (Fig. 7). Those of [13] are slightly shifted to higher frequencies ($\Delta ak_0 < 3$ percent). Katzier used 12 eigenwaves in the waveguide region and six in the scattering obstacle region.

The last testing run presented compares the data of a waveguide to a shielded dielectric image-guide connection [13] (Fig. 8). In the examined range of frequency, the results are also satisfactory (Fig. 9). The ripple at the high end of the frequencies is caused by too coarse a grid distance in the longitudinal direction.

Only one, the basic mode, had to be considered at the cross-sectional planes because these are far enough away from the connecting structure and their lateral dimensions were chosen such that higher modes are evanescent.

The large number of elementary cells in the longitudinal direction could be decreased by including higher modes in the S-matrix calculation because it becomes possible to place the cross-sectional planes nearer to the connecting structure. However, its accuracy has not yet been tested.

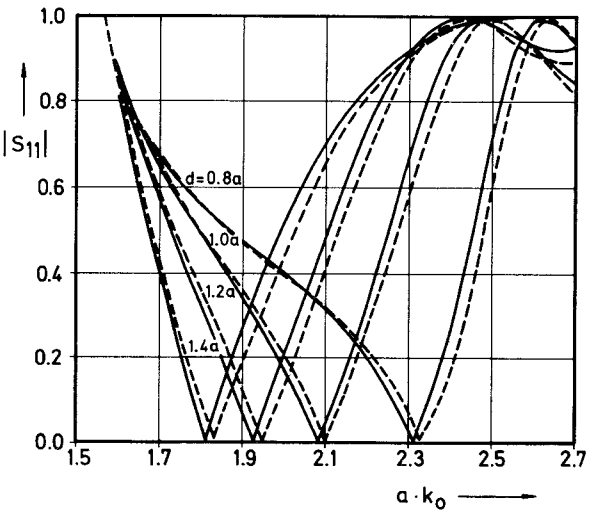

Fig. 7. Magnitude of the reflection coefficient $|S_{11}|$ of the structure of Fig. 6 for different obstacle length d. —— finite-difference method. ----- method of orthogonal expansions [13].

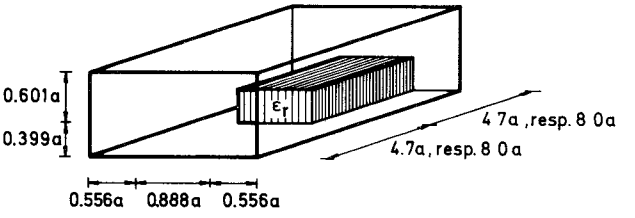

Fig. 8. Waveguide to a shielded dielectric image-guide connection.

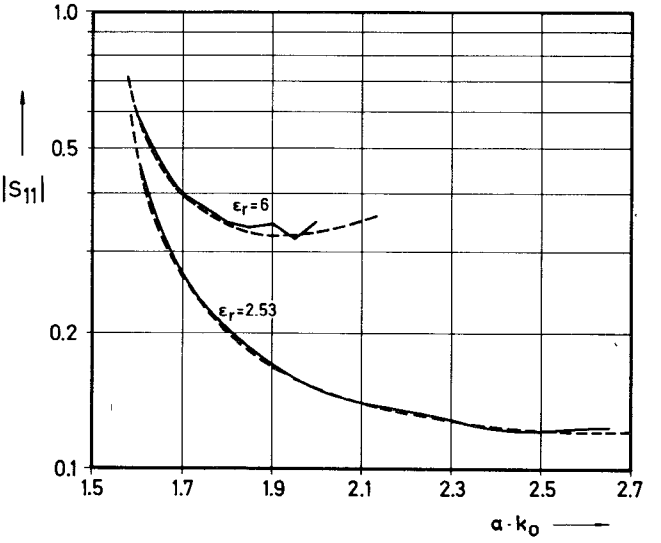

Fig. 9. Magnitude of the reflection coefficient $|S_{11}|$ of the structure of Fig. 8 for different ϵ_r. —— finite-difference method. ----- method of orthogonal expansions [13].

VI. Numerical Results

The interconnection of two microstrip lines, each one on a GaAs chip, has been modeled by an air bridge, by a transition through a dielectric wall (Fig. 10), and by a bond wire (Fig. 17). The magnitude of the S_{11} coefficient and some mode-amplitude sums are plotted. The height of the substrate of the microstrip line is assumed to be 100

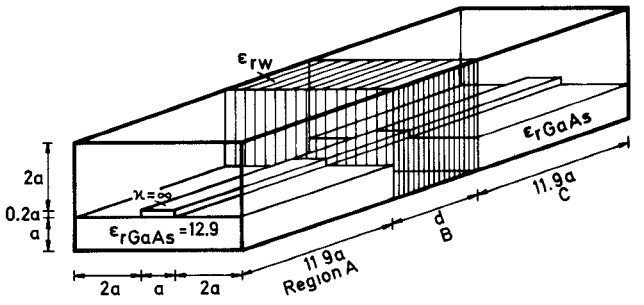

Fig. 10. Interconnection of two microstrip lines by an air bridge and by a transition through a wall, respectively.

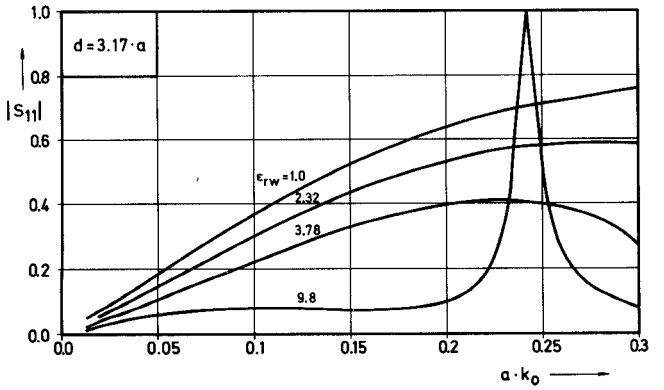

Fig. 11. Magnitude of the reflection coefficient $|S_{11}|$ of the structure of Fig. 10 with $d = 3.17 \cdot a$.

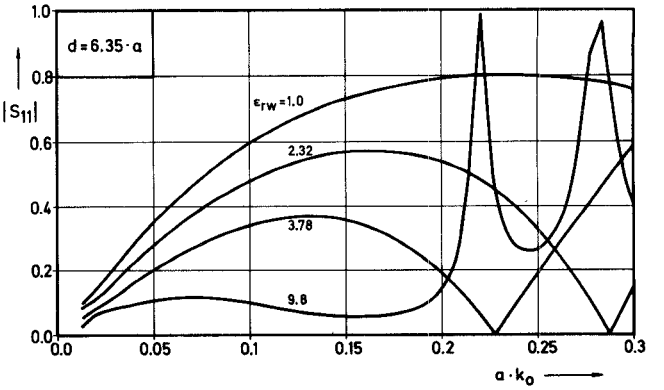

Fig. 12. Magnitude of the reflection coefficient $|S_{11}|$ of the structure of Fig. 10 with $d = 6.35 \cdot a$.

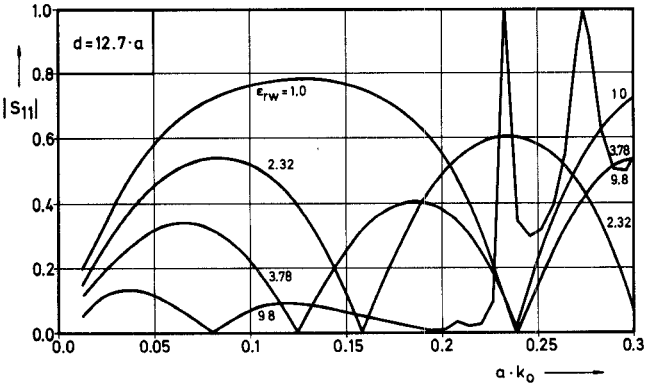

Fig. 13. Magnitude of the reflection coefficient $|S_{11}|$ of the structure of Fig. 10 with $d = 12.7 \cdot a$.

μm, and the conductor dimensions are assumed to be 100 μm$\times$20 μm ($a = 100$ μm). The nonnormalized frequency range is therefore from 6.0 GHz to 143 GHz. It has to be pointed out that other values of the length-normalization constant lead to other frequency ranges (e.g. $a = 0.63$ mm: 0.95 GHz $\leq f \leq$ 22.7 GHz). Also, other substrate materials (e.g. InP) or other dimensions could be chosen for computational runs.

To estimate the accuracy, a microstrip line equal to that shown in Fig. 10 was examined. Its length was equal to that of the longest air bridge structure ($l = 36.5 \cdot a$) and the same grid was used. The maximum of the phase error of the transmission coefficient was $\Delta(\sphericalangle S_{21})_{\max} = 11.3°$ and the maximum of the error of the magnitude of the reflection coefficient was $\Delta|S_{11}|_{\max} = 0.0067$.

Here also, only the basic mode had to be considered, as pointed out at the end of the previous section.

First, the connection via an air bridge ($\epsilon_{rw} = 1.0$) or through a dielectric wall ($\epsilon_{rw} > 1.0$) is examined for different lengths and thicknesses d (Figs. 11–13). Its nonnormalized values are $d = 0.317$ mm, 0.635 mm, and 1.27 mm. The passing of a conductor through a wall is necessary if the device has to be encapsulated. A typical organic dielectric ($\epsilon_{rw} = 2.32$), quartz glass ($\epsilon_{rw} = 3.78$), and ceramics (Al_2O_3, $\epsilon_{rw} = 9.8$) are selected as wall materials.

For small $a \cdot k_0$ or small d, $|S_{11}|$ decreases significantly with an increase of the wall permittivity from $\epsilon_{rw} = 1.0$ to 9.8. This is due to improvement of the matching of the wall to the microstrip lines. Their effective permittivity as a function of frequency was calculated by F2SOLV to be ϵ_{reff} $(a \cdot k_0) = 7.5 \cdots 9.8$. Therefore, particularly for ceramics, the wall is well matched. In contrast, using an air bridge, $|S_{11}|$ rises to about 0.8 for a worst case. Also, $|S_{11}|$ increases for higher permittivity than ceramics.

At high frequencies, two different resonance effects can be observed. The first exhibits a zero reflection characteristic, $|S_{11}| = 0$, the second exhibits a zero transfer characteristic, $|S_{21}| = 0$. In both cases, the structure has to be regarded as a resonator.

The first resonance effect is caused by the destructive interference of the reflected waves at the two microstrip wall planes and has a bandpass-filter property. Its resonance frequencies depend strongly on ϵ_{rw} and d; they are decreasing if ϵ_{rw} or d is increasing. Further, they are shifted to lower values as compared with an unconnected resonator (e.g., $d = 12.7 \cdot a$, $\epsilon_{rw} = 1.0$: $a \cdot k_{0,\text{res, unconnected,1}} = 0.248$, $a \cdot k_{0,\text{res,1}} = 0.238$). This is due to the distortion of the electromagnetic fields at the microstrip wall planes, with the result of the excitation of higher, evanescent modes at both sides. Fig. 14 shows the decomposition of the transverse electric field via the normalized length z of the structure in the case of excitation with equal mode amplitudes at both ends and at the resonance frequency. The mode-amplitude sums of the first and second mode in the regions A, B, and C of the structure are plotted. It can be observed that the half-wavelength of mode B1 is greater than d except if it would be without field distortion.

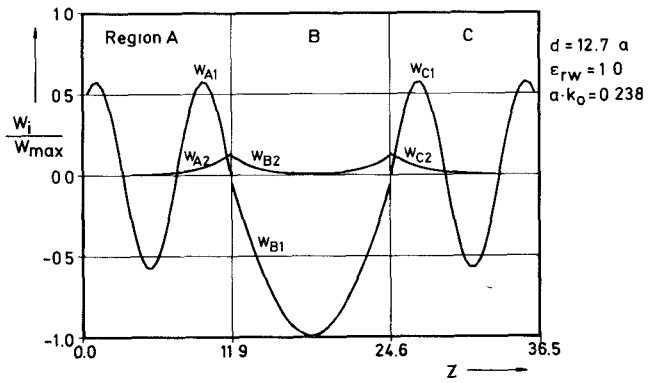

Fig. 14 Normalized mode-amplitude sums w_i/w_{max}, with z the longitudinal structure axis.

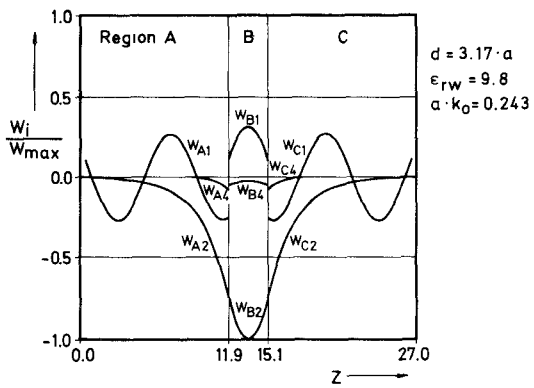

Fig. 15. Normalized mode-amplitude sums w_i/w_{max}.

The second resonance effect has the property of a band-stop filter (e.g., $d = 3.17 \cdot a, \epsilon_{rw} = 9.8$, $a \cdot k_{0,res} = 0.243$). The decomposition of the transverse electric field at the resonance frequency (Fig. 15) shows that the second mode in the wall region (B2) has propagation properties. The field energy is mainly stored in this mode, indicating that the resonance frequency depends on this mode. Being a waveguide mode, it is sensitive to the actual transverse box sizes, i.e., the longer one. In the case under consideration, the resonance frequency is shifted to $a \cdot k_{0,res} = 0.189$ for broadening the box from $b = 5 \cdot a$ to $b = 7 \cdot a$. But an increase in d cannot shift it below the cutoff frequency of the second mode. Notice that the transverse electric field patterns of the second modes in the different regions (A2, resp., C2 and B2) are different. In the vicinity of the resonance frequency, the phase of S_{11} is changed by 180°, and the phase of S_{21} by 360°.

Both resonance effects can be observed for large d and high ϵ_{rw} (Fig. 13). This is the reason for the very sharp increase of $|S_{11}|$ (e.g., $d = 12.7 \cdot a, \epsilon_{rw} = 9.8$, $a \cdot k_0 \simeq 0.23$).

At high frequencies, near but below the cutoff frequency of higher order modes in the connecting structure, their attenuation constant becomes small. Especially for small d, these higher modes contribute to the energy transport (Fig. 16) and influence the electrical behavior. This is obvious by comparing the shape of the $|S_{11}|$ curves with that of the first testing structure (Fig. 5).

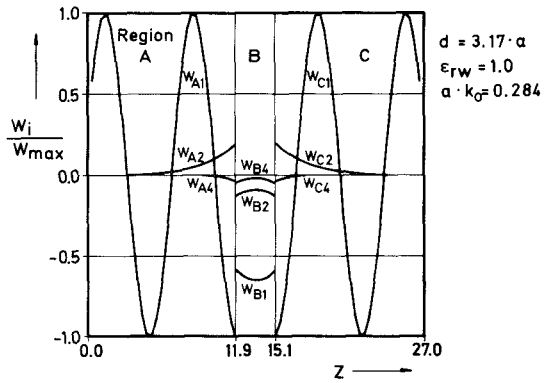

Fig. 16. Normalized mode-amplitude sums w_i/w_{max}.

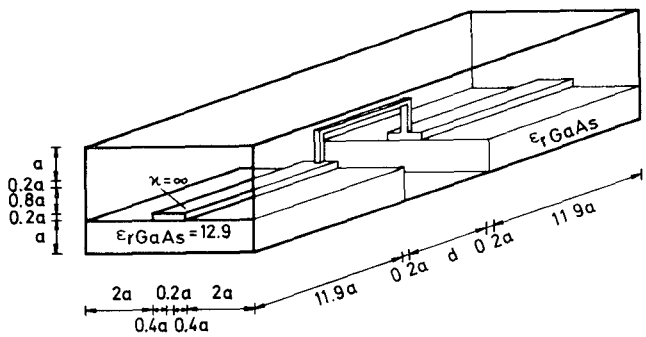

Fig. 17. Interconnection of two microstrip lines by a bond wire.

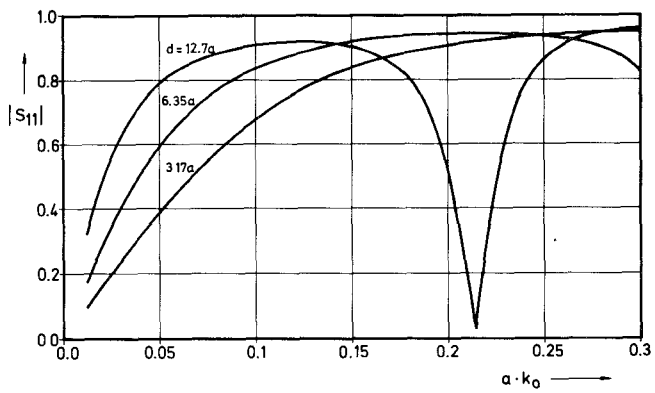

Fig. 18. Magnitude of the reflection coefficient $|S_{11}|$ of the structure of Fig. 17.

The computed results of the interconnection by a bond wire (Fig. 17) are plotted in Fig. 18. $|S_{11}|$ is still higher than that of an air bridge. This is due to a higher inductivity of a small bond wire as compared to a broad conductor bridge. Therefore, the characteristic impedance is higher than that of the air bridge, which itself is higher than that of the microstrip line, meaning deteriorated matching.

A modeling of the electrical behavior of the connecting structures by a T lumped-element circuit with two longitudinal inductance of $L/2$ and a transverse capacitance of C gives quantitative agreement and allows a comparison with measured data given in the literature [5], [6]. The lumped-element values were obtained by optimal fitting of the S_{11} curves (real and imaginary part) in the frequency range $0.02 \leqslant a \cdot k_0 \leqslant 0.075$ using the Levenberg–Marquardt

method. The characteristic impedance of the microstrip line was numerically calculated to be $Z_L = 33\ \Omega$. The inductances obtained for $d = 12.7 \cdot a, \epsilon_{rw} = 1.0$ were $L_{\text{bond}} = 0.70$ nH, which is in good agreement with the literature and $L_{\text{bridge}} = 0.40$ nH. The capacitances, $C_{\text{bond}} = 0.039$ pF and $C_{\text{bridge}} = 0.041$ pF, depend strongly on the frequencies under consideration. With the values given, the fitting is good for small frequencies but not applicable at resonance frequencies.

The bandpass-filter effect appears also using a bond wire, but the resonance frequencies are shifted to lower values as compared with the air bridge.

VII. Conclusions for Design

Three structures were considered in order to interconnect two devices in microstrip technology. A bond wire causes the highest reflections even with relatively low frequencies because of its high inductivity. For a distance of $d = 1.27$ mm, half the energy is reflected ($|S_{11}|^2 = 0.5$) at a frequency $f = 18.6$ GHz.

Therefore, a bond wire is reasonable only for low frequencies. Using an air bridge, this frequency rises to $f = 36.3$ GHz for the same distance. To further increase this, d has to be chosen as small as technologically possible.

Still lower reflections are obtained by a transition through a dielectric wall. This is in any case necessary if the device has to be protected against environmental factors or shielded by metal to suppress radiation or protect against electromagnetic perturbations. Then the conductor has to pass through a dielectric of the type used for coaxial line. By selecting the dielectric, a good matching of the structures is possible; for GaAs microstrip lines, the best material is alumina. To avoid higher propagating modes in the wall, which cause high reflections, the lateral dimensions have to be small. In the case of good matching, the distance d is only of little importance but influences the transverse parasitic capacitance. It rises with d and ϵ_{rw}.

For digital applications where small $|S_{11}|$ and a linear phase for a large frequency range starting at zero are required, the use of short alumina coaxial line connections with small lateral sizes is proposed.

On the other hand, analog applications are mostly of small bandwidth. For frequencies in connection with millimeter-wave circuits, it could then be of advantage to use the first resonance effect ($|S_{11}| = 0$). By choosing ϵ_{rw} and d, its resonance frequency can be shifted to the frequency of interest. Care must be exercised in view of the frequency shifting caused by the evanescent modes and of the dependance of the half bandwidth upon the parameters ϵ_{rw} and d. The technological problem of the required accuracy of d would then be of importance.

Acknowledgment

The authors would like to thank Dr. H. Katzier, Technische Hochschule Darmstadt, for helpful discussions and E. Schnepf, H. Wietschorke, and Dr. P. Weber, all with the Rechenzentrum of Universität Karlsruhe, for their friendly help in connection with the LINSOL program package and the CYBER 205.

References

[1] W. J. Getsinger, "The packaged and mounted diode as a microwave circuit," *IEEE Trans. Microwave Theory Tech.*, vol. MTT-14, pp. 58–69, Feb. 1966.

[2] M. E. Bialkowski and P. J. Khan, "Analysis of diode mounts in millimeter-wave propagating structures," *Arch. Elek. Übertragung*, vol. 38, pp. 227–230, 1984.

[3] M. Maeda, K. Nagano, M. Tanaka, and K. Chiba, "Buried-heterostructure laser packaging for wideband optical transmission systems," *IEEE Trans. Commun.*, vol. COM-26, pp. 1076–1081, July 1978.

[4] P. T. Greiling and R. W. Laton, "Determination of semiconductor junction device package networks," *IEEE Trans. Microwave Theory Tech.*, vol. MTT-22, pp. 1140–1145, Dec. 1974.

[5] R. J. Akello, B. Easter, and I. M. Stephenson, "Experimental measurement of microstrip transistor-package parasitic reactances," *IEEE Trans. Microwave Theory Tech.*, vol. MTT-25, pp. 367–372, May 1977.

[6] H. Beneking, "Comments on 'Experimental measurement of microstrip transistor-package parasitic reactances'," *IEEE Trans Microwave Theory Tech.*, vol. MTT-26, p. 43, Jan. 1978.

[7] N. H. L. Koster and R. H. Jansen, "The microstrip step discontinuity: A revised description," *IEEE Trans. Microwave Theory Tech.*, vol. MTT-34, pp. 213–223, Feb. 1986.

[8] S.-C. Wu and Y. L. Chow, "An application of the moment method to waveguide scattering problems," *IEEE Trans. Microwave Theory Tech.*, vol. MTT-20, pp. 744–749, Nov. 1972.

[9] J. J. H. Wang, "Analysis of a three-dimensional arbitrarily shaped dielectric or biological body inside a rectangular waveguide," *IEEE Trans. Microwave Theory Tech.*, vol. MTT-26, pp. 457–462, July 1978.

[10] R. de Smedt and B. Denturck, "Scattering matrix of junctions between rectangular waveguides," *Proc. Inst. Elec. Eng.*, pt. H, vol. 130, pp. 183–190, Mar. 1983.

[11] A. S. Omar and K. Schünemann, "Scattering by material and conducting bodies inside waveguides, Part I: Theoretical formulations," *IEEE Trans. Microwave Theory Tech.*, vol. MTT-34, pp. 266–272, Feb. 1986.

[12] G. Piefke, *Feldtheorie III*. Mannheim: Bibliographisches Institut, 1977.

[13] H. Katzier, "Streuverhalten elektromagnetischer Wellen bei sprunghaften Übergängen geschirmter dielektrischer Leitungen," *Arch. Elek. Übertragung.*, vol. 38, pp. 290–296, 1984.

[14] J. P. Webb, G. L. Maile, and R. L. Ferrari, "Finite-element solution of three-dimensional electromagnetic problems," *Proc. Inst. Elek. Eng.*, pt. H, vol. 130, pp. 153–159, Mar. 1983.

[15] M. de Pourcq, "Field and power-density calculations by three-dimensional finite elements," *Proc. Inst. Elek. Eng.*, pt. H, vol. 130, pp. 377–384, Oct. 1983.

[16] K. S. Yee, "Numerical solution of initial boundary value problems involving Maxwell's equations in isotropic media," *IEEE Trans. Antennas Propagat.*, vol. AP-14, pp. 302–307, May 1966.

[17] M. Albani and P. Bernardi, "A numerical method based on the discretization of Maxwell equations in integral form," *IEEE Trans. Microwave Theory Tech.*, vol. MTT-22, pp. 446–450, Apr. 1974.

[18] T. Weiland, "Eine Methode zur Lösung der Maxwellschen Gleichungen für sechskomponentige Felder auf diskreter Basis," *Arch. Elek. Übertragung.*, vol. 31, pp. 116–120, 1977.

[19] T. Weiland, "Verlustbehaftete Wellenleiter mit beliebiger Randkontur und Materialbelegung," *Arch. Elek Übertragung.*, vol. 33, pp. 170–174, 1979.

[20] W. Wilhelm, "CAVIT and CAV3D—Computer programs for rf cavities with constant cross section or any three-dimensional form," *Particle Accelerators*, vol. 12, pp. 139–145, 1982.

[21] T. Weiland, "Computer modeling of two- and three-dimensional cavities," *IEEE Trans. Nucl. Sci.*, vol. NS-32, pp. 2738–2742, Oct. 1985.

[22] T. Weiland, "Three dimensional resonator mode computation by finite difference method," *IEEE Trans. Magn.*, vol. MAG-21, pp. 2340–2343, Nov. 1985.

[23] M. Krohne, "Wellenausbreitung und Beugung in einem mit koaxialen dielektrischen Zylindern beschwerten Rundhohlleiter,"

Ph.D. thesis, Technische Hochschule Darmstadt, Darmstadt, West Germany, 1971.

[24] H. Müller, W. Schönauer, and E. Schnepf, "Design considerations for the linear solver LINSOL on a CYBER 205," in *Super-Computer Applications*, A. H. L. Emmen, Ed. New York: North-Holland, 1985, pp. 39–49.

[25] R. Fletcher, "Conjugate gradient methods for indefinite systems," in *Proc. Dundee Biennial Conf. Numer. Anal.*, 1975, pp. 73–89.

✠

Andreas Christ was born in Karlsruhe, West Germany, on May 11, 1958. He received the Dipl. Ing. degree in electrical engineering from the University of Karlsruhe (TH) in 1983. Since then he has been working at the Institute of High-Frequency Techniques at the University of Darmstadt (TH), where he is engaged in the numerical computation of electromagnetic fields applied to embedding problems.

Hans L. Hartnagel (SM'72) was born in Geldern, Germany, in 1934. He received the Dipl. Ing. degree in 1960 from the Technical University Aachen, Germany, and the Ph.D. and Dr. Eng. degrees from the University of Sheffield, England, in 1964 and 1971, respectively.

After working for a short period with the company Telefunken in Ulm, Germany, he joined the Institut National des Sciences Appliquées, Villeurbanne, Rhône, France. He then joined the Department of Electronic and Electrical Engineering at the University of Sheffield, first as a Senior Research Assistant, then (October 1962) as a Lecturer, and later as a Senior Lecturer and Reader. From January 1, 1971, he held the position of Professor of Electronic Engineering at the University of Newcastle upon Tyne, England. Since October 1978, he has been Professor of High Frequency Electronics at the Technical University of Darmstadt, West Germany.

Dr. Hartnagel is the author of books and numerous scientific papers, originally on microwave tubes and later on microwave semiconductor devices, their technology, and their circuits. He has held many consulting positions, partly while on temporary leave of absence from his university positions.